AIAA SciTech
4-8 January 2016, San Diego, California, USA
54th AIAA Aerospace Sciences Meeting

Fabrication of Asymmetric Nanostructures for Plasmonic Force Propulsion

Jaykob N. Maser,[*] Joshua L. Rovey,[†] and Xiaodong Yang[‡], Ling Li[§], Huixu Deng[**]
Missouri University of Science and Technology, Rolla, Missouri 65409

The objective of this research is to manufacture and investigate the characteristics and use of asymmetric, metallic, nanostructures for plasmonic force propulsion, a developing method of nano-/picosatellite thrust generation. Visible to near-infrared light is focused onto sub-wavelength nanostructures to generate polarized oscillations of electrons on the surface of the metallic nanostructures (surface plasmon polaritons). The surface plasmon polaritons accelerate nanoparticle propellant away from the nanostructure, creating thrust. Previous numerical simulations have shown that asymmetric nanostructures can resonate strongly within the visible spectrum. This is the first experiment ever attempted and first to successfully demonstrate this resonance where the resonance peak is λ = 830 nm. The resonance peak of the experimental optical characterization agrees well with our computed model, showing an 11.2% difference. However, the off resonance behavior exhibits peak broadening where the variation of intensity with wavelength, off resonance, has an experimental slope that is 3.7 times less steep than the computed model. Furthermore, the optical transmittance of the sample is 2.1 times higher than computationally modeled. It is shown that the nanostructures are thermodynamically stable in the projected environmental conditions and have an equilibrium temperature of 746.4 K. Upon review of the experimental optical setup, we conclude that thrust generation is not possible with continuous irradiation of light and propose a method of synchronous dynamic acceleration of nanoparticle propellant by use of a pulsed light beam.

I. Introduction

A nano/microsatellite is defined as a satellite in the weight class of 1-50 kg. The demand for and use of these and other small satellites is widespread and is projected to continue to increase according to the 2015 SpaceWorks report on the nano/microsatellite market [1]. The SpaceWorks report also makes note that most nano/microsatellites are launched in large clusters and that certain companies such as SpaceX plan to use large constellations of small satellites for communications purposes. Satellites within sizeable constellations will need the ability to maneuver and orient themselves precisely in relation to the other satellites of the cluster. Coupling these requirements with the constraints of mass and volume demand the use of novel propulsion systems that are optimized for use on smallsats. This propulsion system must also be adaptable for satellites that continue to decrease in size. We investigate the feasibility of a plasmonic force propulsion system to fit this niche.

Plasmonics is a subfield of optics that addresses the nanoscale interactions of light and metallic nanostructures. A metal can be modeled in the following fashion. The atoms within the metal are separated into two parts: a positively charged nucleus and negatively charged electrons. The nuclei are viewed to be fixed in a lattice configuration in which they are restricted in motion whereas the electrons are able to move freely within the metal much like water in a container. This is known as the sea of electrons model. Light can also be split into sub-components: oscillating electric and magnetic fields. An oscillating electric field can impart a force on a charged particle and cause it to move, such as the electrons in the metal that are able to move freely, as stated in the previous model. If a beam of light is allowed to strike the surface of a metal, then the oscillating electric field component of the light will cause the electrons in the metal to oscillate. A group of oscillating electrons is known as a plasmon.

[*] Graduate Research Assistant, Dept. of Aerospace Engineering, 160 Toomey Hall
[†] Associate Professor of Aerospace Engineering, 292D Toomey Hall, AIAA Associate Fellow
[‡] Assistant Professor of Mechanical Engineering, 227 Toomey Hall.
[§] Postdoctoral Research Assistant, Dept. of Aerospace Engineering, 227 Toomey Hall
[**] Postdoctoral Research Assistant, Dept. of Aerospace Engineering, 227 Toomey Hall

Finally, if the metal is restricted in dimensions to the nanoscale regime, the plasmons have the ability to oscillate at the same frequency as the incident light which creates a strong electromagnetic field about the location of the nanostructure. This electromagnetic field can be tuned, by changing the size and shape of the metallic nanostructures, and used to control the motion of particles within the vicinity of the nanostructure. The control of nanoparticles in the vicinity of a plasmon interaction is well known as "plasmon nano-optical tweezers" [2]. This technique demonstrated optical particle trapping coupled with the plasmon interaction to trap nanoparticles at the subwavelength scale.

Our previous research [3] extended this idea of plasmonic nanoparticle manipulation from trapping to acceleration and was specifically aimed at propulsion for smallsats. The plasmonic force propulsion concept is illustrated in Figure 1. A lens is used to focus sunlight onto subwavelength metallic nanostructures that are fabricated to resonantly interact and couple with the incident light which excites surface plasmon polaritons (SPP's) on the metallic nanostructures. The SPP's create a non-uniform electromagnetic force field that causes nanoparticles to be accelerated and expelled from the propulsion device. The nanostructures are attached to the smallsat and the non-uniform field is coupled to the nanostructures by the SPP interaction, therefore the accelerating nanoparticle propellant creates thrust by momentum exchange with the device.

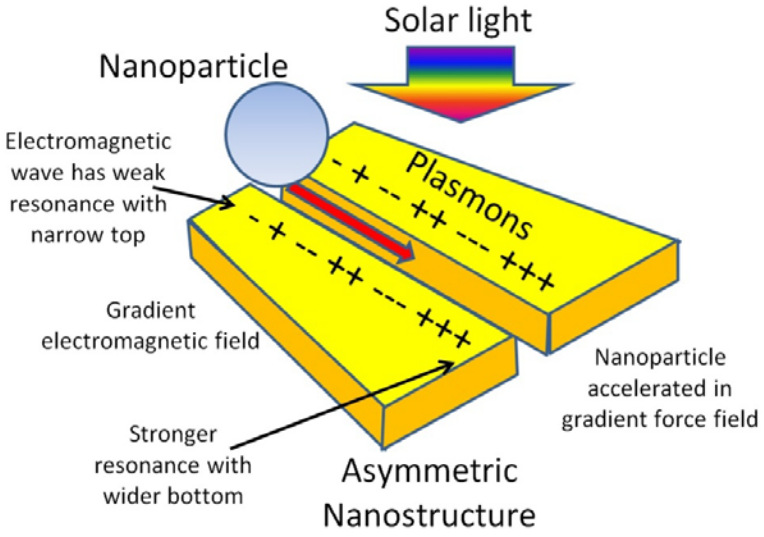

Figure 1: Plasmonic Force Propulsion Concept

The following sections describe an experimental study to investigate the optical characteristics of nanostructures for plasmonic force propulsion. Previous numerical simulations have shown that asymmetric nanostructures can resonate strongly within the visible spectrum. This is the first experiment ever attempted and first to successfully demonstrate this resonance. In the following sections we describe the manufacture of asymmetric nanostructures, their optical characterization, and comparison of experimental results with the numerical simulations. Specifically the experimental and numerical optical transmission spectra are compared. As we will show in Section III, results show that simulations accurately predict the wavelength of strongest resonance but they do not capture the off-resonance behavior. Next the manufacture of asymmetric nanostructures is described, followed by the experiments to characterize the transmission spectrum and compare with numerical simulations. Additionally we present a thermal analysis of nanostructures subjected to solar light to predict the maximum temperature of nanostructures for plasmonic space propulsion. Finally conclusions and future work are presented.

II. Manufacturing Nanostructures

A. Nanostructures for Plasmonic Force Propulsion

In the particle trapping experiments of the "plasmon nano-optical tweezers," symmetric nanostructures are employed [4] because they create symmetric trapping volumes, or potential wells. Therefore, in order to create an asymmetric potential well and strong particle acceleration, asymmetric nanostructures are investigated. An asymmetric, V-groove, type setup was developed by Shalin in 2012 [5] for the one dimensional acceleration and

ejection of nanoparticles out of the V-grooves in a nanocannon fashion. Shalin numerically calculated the maximum exit velocity of particles ejected from these V-grooves to be approximately 11 cm/s in air. They propose that ejection of nanoparticles from the V-grooves will occur due to the gradient force of the *E* field in the grooves and a negative real part of the polarizability of the nanoparticle.

The nanostructure configuration that we chose to use is similar to that of Shalin, an asymmetric assembly. Unlike Shalin's void-type V-groove structure, we use a free-standing structure cut from a film of Au on a substrate of glass. The nanostructures are grouped by two's into a nano-unit. Each nano-unit, Figure 2, is a set of two asymmetric trapezoidal nanostructures where $w = 100\,nm$, $l = 400\,nm$, and $g = 30\,nm$. The geometrical dimensions were chosen such that, based on our previous research, the nano-unit would resonate strongly within the solar spectrum, specifically at a wavelength of 830 nm [3].

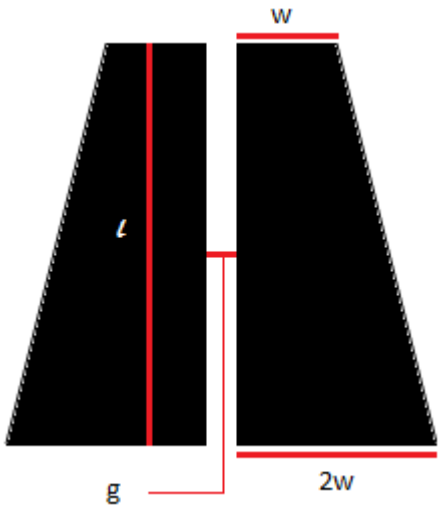

Figure 2: Geometry of a Nano-unit Comprised of Two Trapezoidal Nanostructures

In our previous research [3] we investigated and presented the motivation for our choice of this trapezoidal configuration. Desirable characteristics include a surface plasmon resonance within the 400-1100 nm band of solar light so that we could investigate its use for satellite propulsion. The geometry also needed to create a gradient opto-electromagnetic force field along the length of the nano-unit so that particle ejection could be investigated. The choice of this configuration was also motivated by the desire to obtain two dimensional precision in the direction that the nanoparticles are expelled rather than the one dimensional ejection of Shalin's group. Furthermore, fabrication of free-standing structures from a Au film on a substrate is reasonably accomplished by use of a focused ion beam (FIB).

The metallic nano-units have a specific resonance band in which surface plasmon polaritons are excited. This resonance/absorption band, which is dependent upon the size of the nanostructure, can be determined by computationally modeling the system. We used COMSOL Multiphysics to model the gradient optical force produced by the nanostructures upon resonant excitation by integrating Maxwell's stress tensor of the Lorentz force, Figure 3 [3].

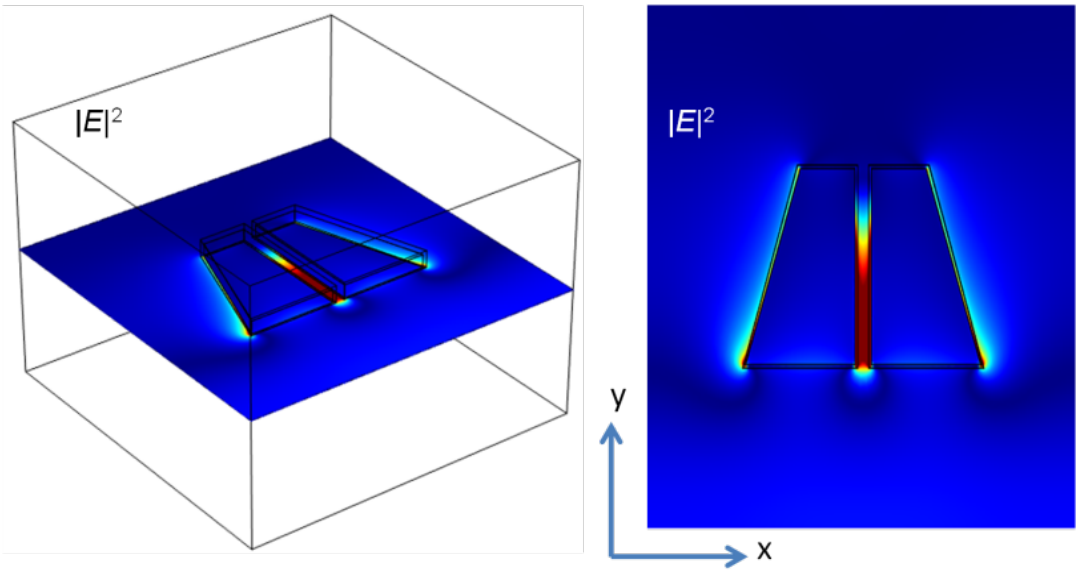

Figure 3: COMSOL Multiphysics Simulation of Solar Light Excitation of Asymmetric Nano-unit

The computed transmission spectrum for a nano-unit, with the dimensions given in Figure 2, is displayed in Figure 4 where we can see that the resonant wavelength is approximately 845 nm. It was assumed that the nano-unit was irradiated with horizontally polarized light, or light polarized along the width of the nano-unit. The red-shaded box in Figure 4 indicates the wavelengths over which we can gather experimental data with our experimental equipment.

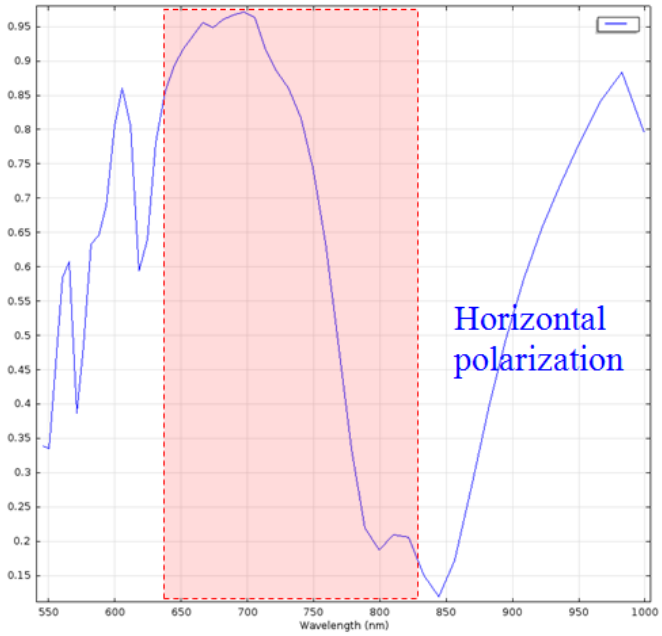

Figure 4: Computed Transmission Spectrum of the Nano-units

B. Manufacturing Process

The nano-unit described above was replicated to form a repeating array. The sample that the repeating array was milled from was a thin film of Au, approximately 30 nm thick, deposited on a glass substrate. The focused ion beam (FIB) on the FEI Helios Nanolab 600 Dualbeam SEM/FIB was used to mill the negative area of the pattern and

leave behind the freestanding nanostructures. Many parameters were altered to determine the operating conditions that produced the array of structures that had the best fit to the theoretical template. A high accelerating voltage (30 kV) was combined with a low beam current (9.7 pA) so that each gallium ion from the beam would have enough energy to mill away the sample but there would be few enough ions hitting the sample that the pattern to be milled would not become washed out. The ion beam has a specific focal point measured to the center of the image area. As the beam moves to the edges of the image area, the beam strikes the sample at an increasingly non-perpendicular value. This change in incident angle increases the distance from the exit point of the beam at the column to the impact point of the beam on the sample surface. Therefore the beam can become out-of-focus at the edges of an image even if dynamic focus is used. A beam that is out-of-focus will produce patterns that have very low quality; the error of the manufactured pattern in relation to the theoretical template will be large. This effect can also occur if fabrication of too large an array is attempted. To stymie this, a large array of 50x50 nano-units was constructed by sequentially milling sets of 10x10 arrays adjacent to each other. Fabrication of a large array of 50x50 nano-units was necessary so that the physical dimensions of the entire array would be comparable to the optical beam that was used to experimentally determine the resonant wavelength of the array.

C. Manufacturing Results

A good quality SEM image is one in which the features are distinguishable, specifically any edges in the image, and is in focus. This is true for FIB patterns and images as well. A good run of fabrication with FIB produces patterns that have distinguishable features and are not washed out, which is caused by having a poorly focused FIB. The progression of quality of our fabricated patterns shows evidence of the improvement in the fabrication process (Figure 5). Focusing the FIB can be difficult because to focus the beam it must be on but when the beam is on, even at a low ion current, it causes damage to the sample. Experience in focusing the beam quickly but sufficiently is necessary.

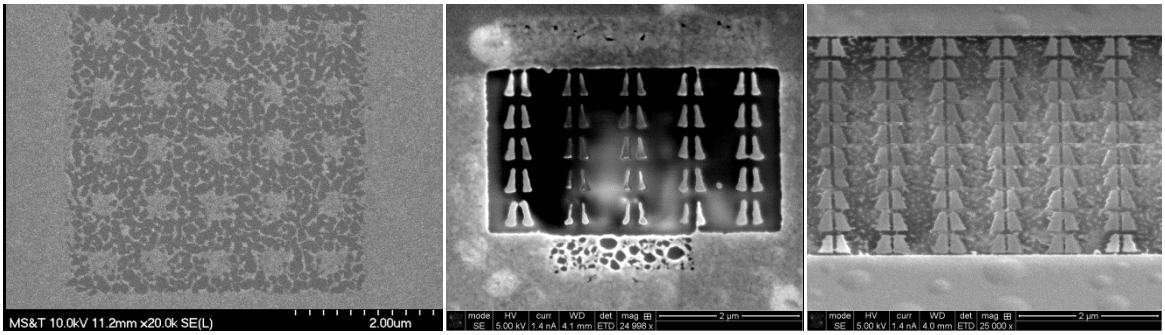

Figure 5: Quality Progression (left to right) of Array Fabrication

A 50x50 nano-unit array (Figure 6), with the dimensions described in Figure 2, and an inter-nano-unit spacing of 50 nm gave an overall array dimension of 24 μm by 22.5 μm. A subsection of this array, which was also used for optical characterization, is pictured in Figure 7.

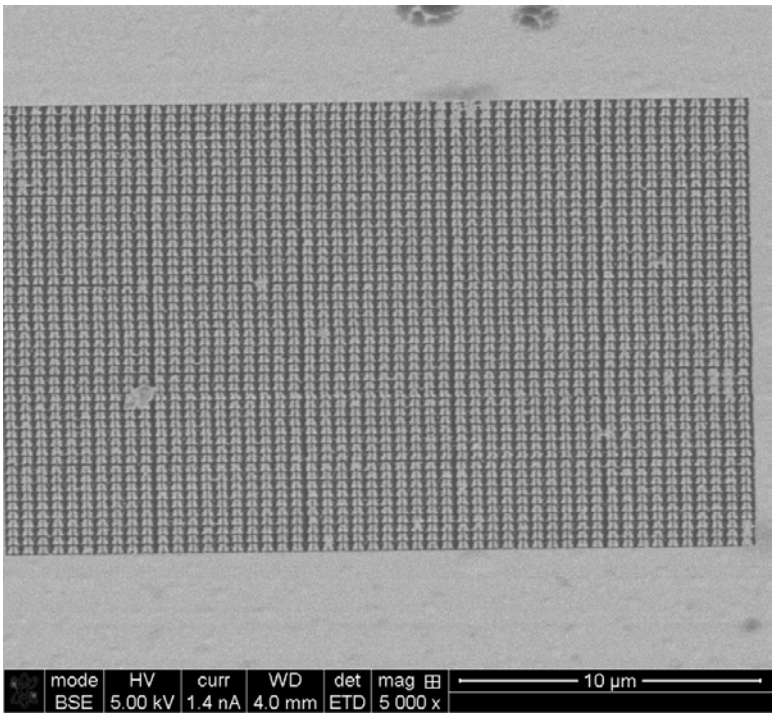

Figure 6: Image of the 50x50 Nano-unit Array

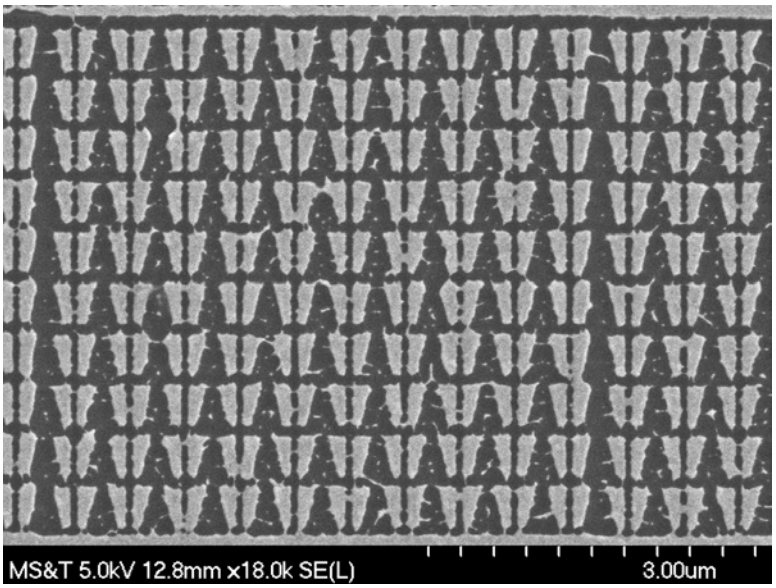

Figure 7: Subsection of the 50x50 Nano-unit Array Used for Optical Characterization

Fabricated nanostructures were compared with the theoretically desired nanostructure array pattern to determine the array that had the least amount of error between the template and the manufactured sample. Images of each array were taken using the scanning electron microscope (SEM) on the above FEI system. Due to the glass substrate, heavy charging occurred throughout the array after milling took place, therefore steps were taken to reduce charging. Copper tape was attached from the gold film to the pin stub that held the sample and images were taken using backscattered electrons rather than secondary electrons. A large negative bias voltage (-150 V) was placed on the Everhart-Thornley detector so that only backscattered electrons, which have the energy of the beam, were detected. Since backscattered electrons have such high energy, the observed charging effects of the sample were

minimal, if not inconsequential. Obtaining images of an array allowed each nanostructure to be measured and the roughness, a measure of the variation of each data point along an edge from its expected value, to be calculated. The approximate edge of each nanostructure was determined by finding the greatest change in pixel value of the image at the location of the nanostructure edge within the image. Then the dimensions of the nanostructures were determined by using the approximate edges that were found. The error, or roughness, along each edge of the nanostructures was determined by calculating the distance between the approximate edge and where the edge should be. The sum of these values was then taken using the Mean Absolute Error: the following equation.

$$MAE = \frac{1}{n}\sum_{i=1}^{n}|f_i - y_i| \tag{1}$$

A set of operating conditions that produced the highest accuracy nanostructures was then chosen by minimizing the roughness of the edges of the nanostructures. Using equation (1), we were able to track the error for each set of operating conditions in the fabrication process. Figure 8 displays the error between the fabricated array and the model versus the type of electron detector used.

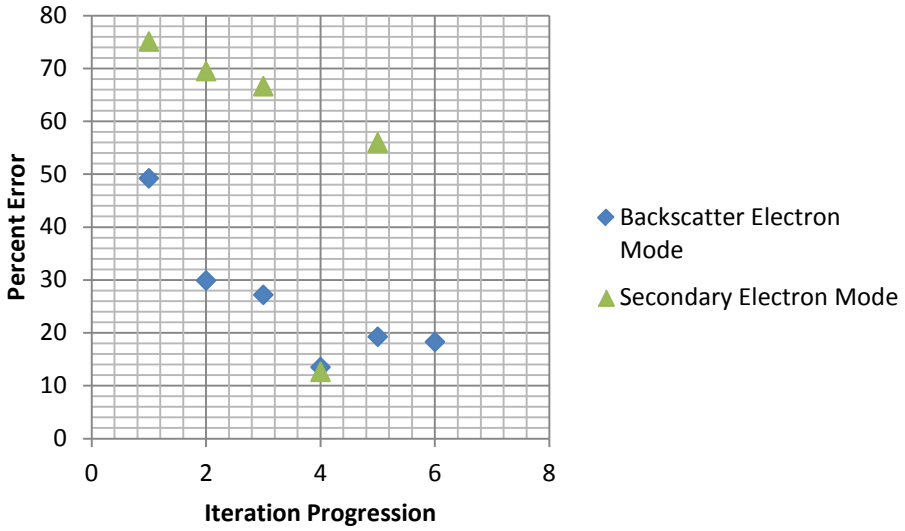

Figure 8: Observed Error Using Different Detection Modes

There are primarily two types of electrons that can be detected once they have interacted with the sample: 1) a backscattered electron and 2) a secondary electron. A backscattered electron is an electron that originated from the beam and has been deflected by an angle greater than 90° out of the sample. This type of electron maintains the energy it had from the beam (5 – 30 kV) therefore any accumulated surface charge on the sample will have little effect on it. A secondary electron is an electron that has been excited and ejected from the sample. It has a much lower energy (100's of eV max) and is therefore greatly affected by any sample charge accumulation. A mixed mode detector gathers data from both types of electrons while a backscatter electron detector and a secondary electron detector primarily register their respective electrons. If Figure 8, we see that high observed error accompanies the use of the secondary electron mode. This is expected due to the ease at which a secondary electron is affected by accumulated sample charge. When affected by sample charging, the secondary electrons can cause image streaking, mirror effect (where incident electrons are reflected by accumulated charge rather than the sample surface) and even sample drift. These possibilities lead us to the conclusion that the use of a backscatter electron detector would be more accurate, which is supported by the data in Figure 8 and the images in Figure 9.

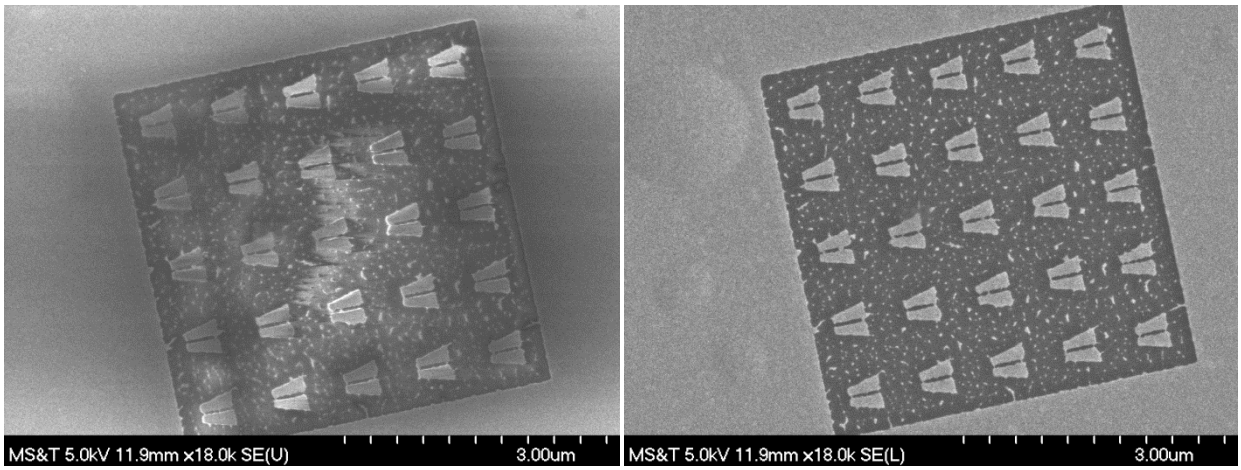

Figure 9: (left) Image Acquired Using Secondary Electron Detector, and (right) Backscatter Electron Detector. **Mild sample charging and image streaking are observed near the upper right of the left array/image.**

It was difficult to determine how each parameter affected the quality of the fabricated structures because the resolution, or quality of focus, of the ion beam when undergoing fabrication was, by far, the deciding factor. If the focus was poor, then structures like those in the first image of Figure 5 were created whereas those in the last image were made if the focus was tuned precisely. This factor is difficult to quantify due to its dependence on the operator. Even though the resolution of the ion beam was the predominant influence on the quality of the nanostructures, the influence of other variables on the nanostructure quality were tracked as well. Figure 10 shows the percent error as it depends on the electron beam current. We would expect that the larger beam current of 10 μA would cause heavy sample charging rather than the 1.4 nA current but we suspect that the higher energy backscattered electrons overcame any charging effects in the 10 μA beam current case and conclude that data accumulation of a broader range of beam currents with each detection method is necessary for further comparison.

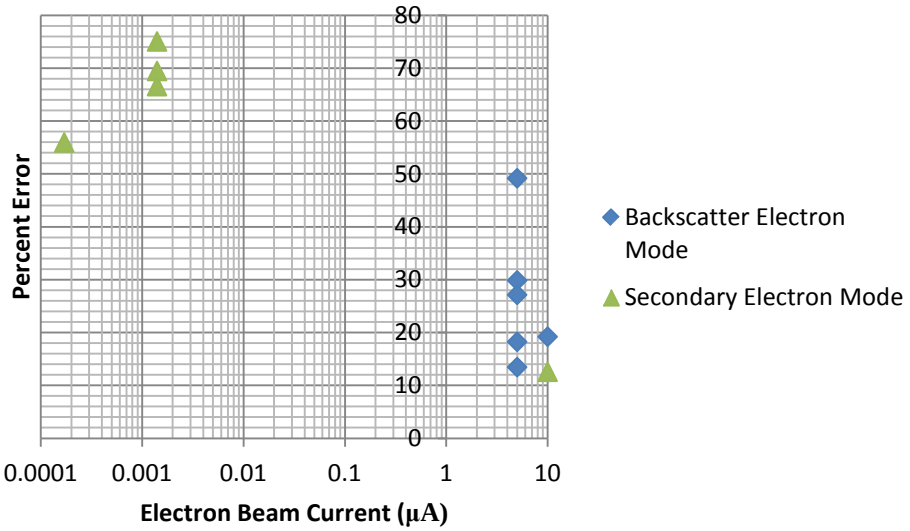

Figure 10: Observed Error as the Electron Beam Current was Varied for Different Detection Modes

III. Characterization of Nanostructure Optical Transmission

We have presented the computed optical transmission spectrum of the modeled nano-unit assembly above in Figure 4. An experimental determination of the actual transmission spectrum of the fabricated nano-units is performed. Due to the error in the nano-unit arrays from the fabrication process, it is expected that peak broadening

of the resonance will occur and that the on resonance absorption will be slightly diminished. In this section, we will describe the experimental setup of the optical characterization scheme and present the results that were obtained.

A. Experimental Setup

An incoherent, Halogen, white-light source was focused onto the array to mimic Sun light and a Horiba spectrometer with a CCD detector was used to measure the intensity of light transmitted through the array. The expectation for this test is that the transmission of all wavelengths will be high except for the transmission of light with a wavelength of approximately 830 nm. The transmission of 830 nm light should, ideally, be zero. This would mean that the 830 nm light resonated with the nano-units and the energy from this band of the incident light was used to produce a strong, gradient electrical-optical force field. To show this, the light source was turned on and focused through a Nikon microscope to illuminate the sample. The spectrometer was then used to scan through the wavelengths produced by the source to measure the transmission of the source light.

B. Experiment Results and Comparison of Experiment with Numerical Predictions

Figure 11 shows the experimental results of the optical characterization of the array, normalized to the intensity of the unobstructed beam.

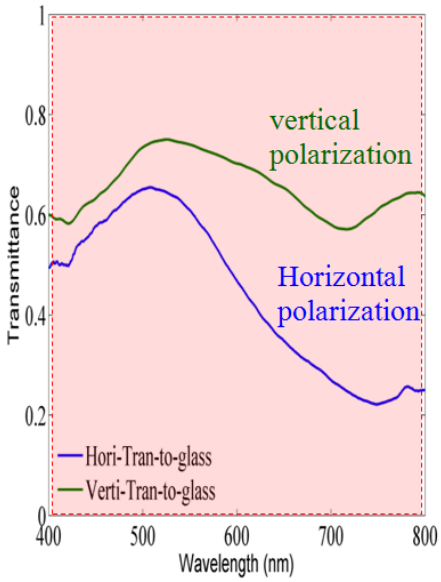

Figure 11: Experimental Results of Optical Characterization

We see from a comparison of Figure 4 and Figure 11 that the difference between resonance locations of the experimental characterization, ~750 nm for the horizontally polarized light, and the computed resonance, ~845 nm, is 11.2 %. The difference in resonance location is likely due to the error in nanostructure dimensions between the modeled nano-unit and the experimentally fabricated nano-unit because the surface plasmon resonance is size dependent. Further comparison of the two figures shows that the energy transmittance of the experimental sample is 2.1 times higher than the computed model. We also see from the computed transmission spectrum that the form, or the trend, of the spectrum is similar for both the computed model and the experiment but the off resonance behavior doesn't follow exactly. The rate of change of the resonance peak, which determines the wavelength selection precision, is 3.7 times steeper in the computed model than in the experimental characterization. This means that the experimental characterization experiences peak broadening. Better agreement between the computed model and the experiment can be achieved by further reducing the fabrication error of the nanostructures. Two polarization schemes of the incident light were tested in the optical characterization. We see that the horizontally polarized light has a stronger resonance than the vertically polarized light. Further investigation can show whether or not the shape of the potential profile of the nano-units depends on the percent absorbance or if the amount of energy converted into plasmons simply changes the depth of the potential. As seen in the experimental characterization, resonance with the incident light is polarization dependent; therefore, if the potential profile is resonance dependent, it could be possible for the potential profile to be tuned by changing the polarization of the incident light, thereby changing the trapping location of nearby nanoparticles.

IV. Nanostructure Thermal Analysis

Calculations to determine the thermal stability of the nanostructures under the incident light were also performed in order to ensure that the nanostructures would not melt at the necessary operating conditions. The amount of energy required to melt the Au nanostructures is determined and compared to the amount of energy radiated away from the nanostructures.

A. Model Description

The model that we have developed to determine whether or not the Au nanostructures will melt is a simple calculation of the change of states of a material and how much energy is required to undergo this change. Then, the Stefan-Boltzmann law is used to calculate the amount of energy that would be radiated from a blackbody radiator representative of the Au nanostructures. The amount of energy needed to raise m grams of Au ΔT degrees Celsius is given by equation (2). Subsequently, equation (3) is used to determine the amount of energy needed to convert m grams of Au from the solid phase at the melting temperature, T_m, to the liquid phase, where c is the heat capacity and L_f is the latent heat of fusion.

$$\Delta Q = cm\Delta T \tag{2}$$

$$\Delta Q_f = L_f m \tag{3}$$

Mass is determined by taking the density of gold times the volume of the nanostructure, equation (4). For these calculations, one nanostructure is defined as one trapezoidal structure. A nano-unit, which produces the plasmonic force, is defined as two of these trapezoidal structures in close proximity to each other.

$$m = DV = 19.32\frac{g}{cm^3} * 1.8 * 10^{-15} cm^3 = 3.478 * 10^{-14}\, g \tag{4}$$

Using numbers for Au in equations (2) and (3), we get the total energy needed to melt m grams of Au, equation (5).

$$\Delta Q_{tot} = \Delta Q + \Delta Q_f = cm\Delta T + L_f m \tag{5}$$

$$\Delta Q_{tot} = 0.129\,\frac{J}{g\cdot ℃} * 3.478 * 10^{-14} g * \left(1064℃ - (-273.15℃)\right) + 63\frac{J}{g} * 3.478 * 10^{-14} g$$

$$= 5.99928 * 10^{-12} J + 2.19114 * 10^{-12}\, J$$

$$= 8.19 * 10^{-12}\, J$$

To determine the amount of energy that is transferred to the nanostructure from the incident sunlight, the ratio of the surface area of the nanostructure to the spot size of the incident light is used. The irradiance of 800 nm sunlight, in low earth orbit, is approximately 1.1 W/m^2. If the irradiance is multiplied by the area of the magnifying lens, then the total incident energy focused at the image of the lens can be determined. This value is then divided by the area of the image to determine the energy density of the incident light at the focus. Finally, this new energy density is multiplied by the cross-sectional surface area of a single nanostructure to determine the total incident energy on a single nanostructure. This can all be condensed into one equation, equation (7). The area of the image created by the magnifying lens is calculated using equation (6), where half the width of the propulsion device and half its length is used to determine the hypotenuse from the center of the device to one of its corners. This is necessary because the image will be circular and it will need to encompass the entire array to irradiate each nanostructure.

$$r = \sqrt{\left(\frac{5}{2} * 10^{-3} m\right)^2 + \left(\frac{52}{2} * 10^{-6} m\right)^2} = 2.5 * 10^{-3}\, m$$

$$A_I = \pi(2.5 * 10^{-3} m)^2 = 1.96 * 10^{-5}\, m^2 \tag{6}$$

$$P_{ns} = P_I \frac{A_{ns}}{A_I} = I_{leo} \frac{A_{lens} A_{ns}}{A_I} \tag{7}$$

$$= 1.1\frac{W}{m^2}\frac{\pi(5 * 10^{-2} m)^2 (1.5 * 100 * 10^{-9} m * 400 * 10^{-9} m)}{1.96 * 10^{-5} m^2} = 2.64 * 10^{-11}\,\frac{J}{s}$$

The nanostructure radiates energy in addition to absorbing it. Therefore, if no energy in the system goes to interactions such as the creation of plasmons and only to radiation, the Stefan-Boltzmann law can be used to calculate how much energy is radiated, equation (8).

$$P_{rad} = \varepsilon A_{ns}\sigma\left(T^4 - {T_e}^4\right) \tag{8}$$

ε is the emissivity of the material and σ is a constant. T_e is the temperature of the environment, taken to be zero in this case and T is the temperature of the material, taken to be T = 1337.15 which is the temperature that Au melts.

$$P_{rad} = 0.025 * 1.5 * 100 * 10^{-9}m * 400 * 10^{-9}m * 5.67 * 10^{-8}\frac{W}{m^2K^4} * 1337.15^4\ K^4$$
$$= 2.72 * 10^{-10}\ \frac{J}{s}$$

B. Model Predictions

The model predicts that the energy radiated by the nanostructure is greater than the energy absorbed by it; therefore the nanostructures will not melt. The bulk melting temperature of Au was used in the calculations. This assumption is reasonable because, even though nanoparticles have a lower melting temperature than their bulk counterpart, Au does not exhibit a significantly lower melting temperature for particles larger than 10 nm radius [6]. Since the amount of energy radiated away from the nanostructures is larger than the amount of energy absorbed by them, we can set the amount of energy absorbed by the nanostructures as P_{rad} in equation (8) so that we can solve for the equilibrium temperature that the nanostructures will reach. Doing so gives us a nanostructure temperature of $T_{nano} = 746.4\ K$.

V. Synchronous Dynamic Acceleration of Nanoparticles

We found that acceleration and emission of nanoparticles would not occur under continuous irradiation, therefore we investigate the use of pulsed light to create a dynamic acceleration of the nanoparticles. With proper timing, nanostructures can be excited and de-excited such that nanoparticles are always being accelerated. This technique is described and further characterized next.

A. Continuous Excitation of Nanostructures

The potential profile that was originally computed for the nano-unit assemblies, Figure 12, was revisited and has led to our understanding that the profile is in fact a potential well that returns to zero. This follows from a simple understanding of the conservation of energy that any potential must return to zero at an infinite distance from the source.

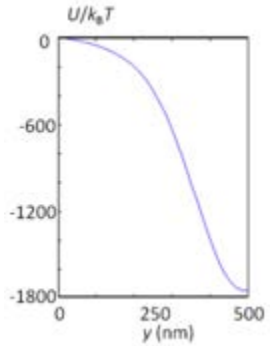

Figure 12: Potential Profile of a Nano-unit

Since the potential is a well, constant irradiation as proposed previously would cause trapping of the nanoparticles rather than acceleration and expulsion. This led us to develop and investigate other theories to cause the particles to be accelerated away from the nano-units. One possible way to accelerate and expel nanoparticles is to pulse the light source, that is, to provide dynamic excitation to the nanostructures. With the constant light source,

trapping would occur in a location other then the center of the nano-unit which may prove to be useful in other applications but, in this instance, acceleration is the preferred response.

B. Dynamic Excitation of Nanostructures and Acceleration of Nanoparticles

This theory maintains a constant pulse length of the incident light, both the on and off modes, and changes the path length of each acceleration stage so that one light pulse can synchronously accelerate each nanoparticle located at every acceleration stage. The main question we seek to address in investigating this theory is whether or not the total length of the assembly will be of a reasonable scale to maintain the application of this nanoparticle accelerator as a propulsion device for smallsats. We answer this question by calculating the total length it would take for a nanoparticle to be accelerated from rest to 1 m/s.

1. Overview of Dynamic Excitation of Nanostructures

If the incident light is pulsed in a way that allows the nanoparticle to initially accelerate down the potential in Figure 12 then travel at a constant velocity away from the structure when the nanoparticle reaches the minimum of the well, the nanoparticle may not feel a force acting against its motion and can be expelled as propellant. This will occur if the light pulse irradiates the nano-unit while the nanoparticle travels the distance from the start of the potential well to the minimum of the well then the pulse turns off while the nanoparticle travels the distance to the beginning of the potential of the next nano-unit in a multistage array. When the light pulse is on, the nanoparticle feels a force that pulls it towards the minimum of the potential well but when the pulse is turned off the potential well is destroyed and the nanoparticle no longer feels a force; therefore it continues in motion under constant velocity. As the nanoparticle proceeds through progressive stages of acceleration its velocity increases, this means that the distance the particle travels while the light beam is off must also increase so that the timing of the light pulse can remain constant. If the pulse width of the light beam was altered rather than the separation distance between acceleration stages, nanoparticles would be out of phase with each other when they arrived at new acceleration stages so that when the light pulse turned on to accelerate one nanoparticle it would hinder the motion of another nanoparticle because the second nanoparticle may not be in the constructive acceleration zone of an acceleration stage.

2. Model of Dynamic Excitation

The dynamic excitation model is constructed by calculating the amount of acceleration that a nanoparticle would feel from a single nano-unit stage. This acceleration value will be the same for each stage, therefore we can 1) calculate the exit velocity of a nanoparticle from a single stage, 2) use this velocity to determine the distance the nanoparticle travels while the light pulse is off, 3) also use this velocity as the initial velocity into the next acceleration stage, and 4) iterate this process until the desired velocity is obtained. Then we can review the device parameters that are required to achieve that velocity such as the total length of the device and the number of nano-unit stages needed to accelerate the nanoparticles to the desired velocity.

The repulsive force profile is given in Figure 13 and an accompanying polynomial is fitted to it, equation (9).

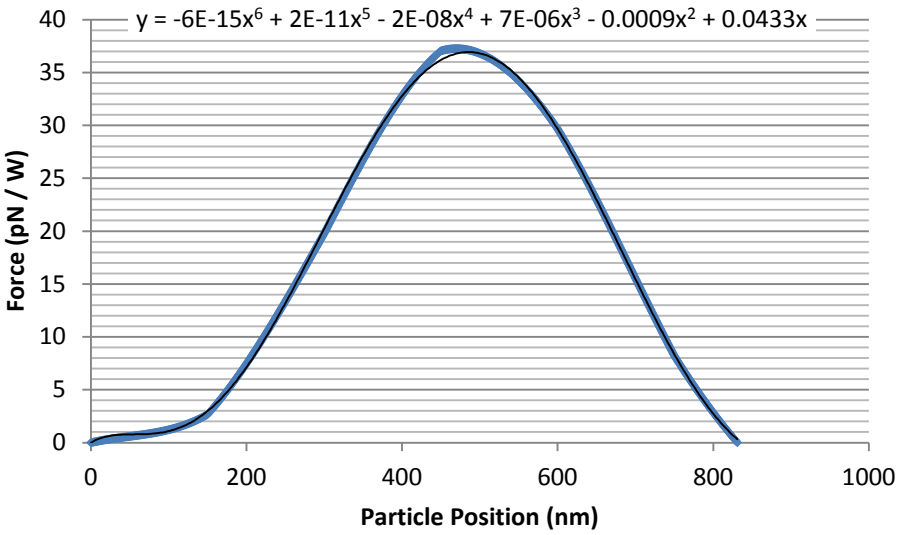

Figure 13: Repulsive Force Profile of a Single Nano-unit

$$y = -6 * 10^{-15}x^6 + 2 * 10^{-11}x^5 - 2 * 10^{-8}x^4 + 7 * 10^{-6}x^3 - 9 * 10^{-4}x^2 + 4.33 * 10^{-2}x \quad (9)$$

The total repulsive force acting on the nanoparticle per watt of input energy is found by taking the integral of equation (9), where the negative sign indicates that it is a repulsive force.

$$F_{tot} = \int_0^{831} y dx = -4.47 * 10^4 \frac{pN}{W} \quad (10)$$

Then the actual force from the nano-unit acting on the nanoparticles can be determined, equation (13), by factoring in how much energy the nano-unit absorbs at its resonance frequency. Say there is incident light, representative of solar radiation, of ~ $1\frac{W}{m^2}$ at a wavelength of 800 nm, the approximate resonant wavelength of the test structure. Then the energy absorbed by the nano-unit is seen in equation (12), given that its area is found in equation (11).

$$A_{nano} = 2 * \left(\frac{3}{2} * 100 * 10^{-9}m * 400 * 10^{-9}m\right) = 1.2 * 10^{-13}m^2 \quad (11)$$

$$P_{nano} = 1.2 * 10^{-13}W \; at \; 800 \; nm \quad (12)$$

$$F_{nano} = F_{tot} * P_{nano} = -5.364 * 10^{-9} \; pN \quad (13)$$

The change in velocity of the nanoparticle due to one nano-unit can be determined simply by dividing the actual force from the nano-unit by the mass of the nanoparticle, which was determined from the volume of a polystyrene nanosphere with radius r = 50 nm.

$$a_{nano} = \frac{F_{nano}}{m} = \frac{-5.364*10^{-21}\,N}{5.45*10^{-19}\,kg} = 9.84 * 10^{-3} \; \frac{m}{s^2} \quad (14)$$

If the nanoparticle is assumed to have no initial velocity, then the velocity it has after passing over one nano-unit is

$$v_{f_1} = \sqrt{2a_{nano}\Delta x} = 1.28 * 10^{-4} \; \frac{m}{s} \quad (15)$$

where $\Delta x = 831 \; nm$. We can now choose a shutter speed for the light pulse such that the incident light beam is blocked while the nanoparticle travels between nano-units where the distance between nano-units is $\Delta x = 200 \; nm$ in this case.

$$t_{sh} = \frac{\Delta x}{v_{f_1}} = .0016\ s \tag{16}$$

200 nm is arbitrarily chosen so that the interactions of the surface plasmon resonance of one nano-unit do not interfere with the interactions of the surface plasmon resonance of another nano-unit in the acceleration path of the nanoparticle.

3. Model Results and Predictions

Using the values that have already been calculated and computationally iterating the motion and velocity of the nanoparticle, the acceleration length of the system can be determined, Figure 14.

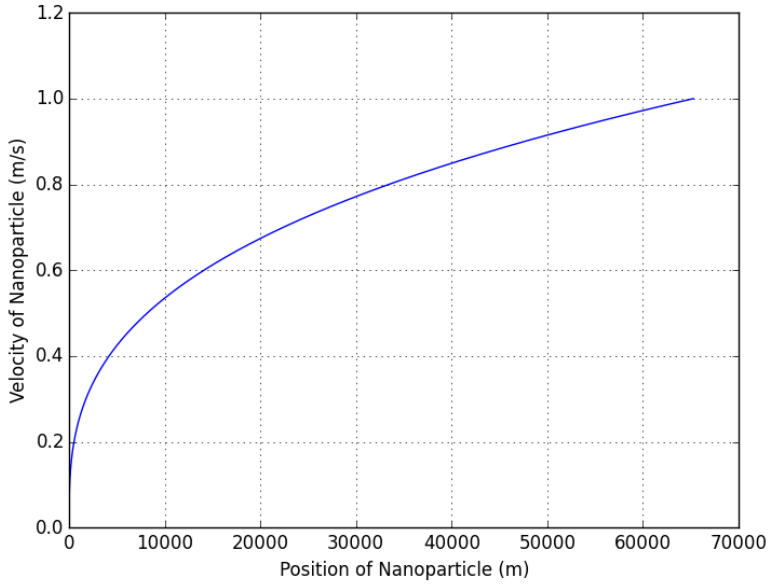

Figure 14: Position of Nanoparticle as its Velocity Increases

Figure 14 shows that the nanoparticle experiences diminishing returns as its velocity increases, such that a larger distance and increasing iterations of nano-units must be met to gain equivalent increases in velocity. It takes the nanoparticle 7 cm to accelerate an order of magnitude from 1 mm/s to 1 cm/s but it takes 7.1 km for the nanoparticle to double its speed from 0.25 m/s to 0.5 m/s. For the nanoparticle to reach a velocity of 1 m/s, it takes a total acceleration path length 65.3 km.

4. Conclusions Regarding Dynamic Excitation and Acceleration of Nanoparticles

To remedy the trapping attribute of the nano-units when held under constant illumination a pulsed beam of incident light was considered. Although a pulsed light beam would cause the nanoparticles to accelerate and be propelled away from the system, sufficient particle velocities would be achieved within distances too large for the application of this system as a micro/nano-sat propulsion device. Application as a novel, ground-based, linear accelerator may have use in other areas of research.

VI. Conclusion

By way of the manufacturing process, we found that certain operating parameters increased the quality of our fabricated nanostructures. We determined that charge accumulation on the sample was inevitable due to the glass substrate and that low beam currents such as 10 μA, when using the backscatter detector, or 1.4 nA, when using the secondary electron detector, helped in reducing the observed charge accumulation. We concluded that use of the backscatter electron detector produced images with half the observed manufacturing error (avg. 26.2 %) than images produced with the secondary electron detector (avg. 55.9 %). We also concluded that the quality of the nanostructures is highly dependent upon the resolution of the FIB, which is a qualitative parameter.

The optical characterization was successful in accurately demonstrating the surface plasmon resonance peak of the trapezoidal nanostructures but lacked off-resonance agreement. Due to non-ideal nanostructures, the transmission spectrum was slightly blue-shifted and greatly decreased in the percent transmittance from 11% on-resonance transmission in the computed result to approximately 25% on-resonance transmission in the experimental characterization. We observed that the resonance location agreed with the computed model with an error of 11.2% but that the off resonance characteristics were much less predictable with a slope 3.7 times steeper in the computed model. We also observed that the polarization of the light may change the potential profile of the plasmon resonance which we plan to investigate further. Polarization dependent dynamics of nanoparticles trapped by surface plasmon resonant interactions has been observed already in Tsai's work [7].

We concluded in the thermal analysis of our nanostructures that the structures would be able to withstand the operating conditions of the environment that would be necessary if they were to be used as a smallsat propellant system. Specifically, the nanostructures would not melt under the irradiation of Solar light. Instead, their temperature will reach an equilibrium maximum at $T_{nano} = 746.4\ K$.

Finally, in the dynamic excitation modeling we developed, investigated, and presented a method to achieve nanoparticle acceleration with the surface plasmon resonance setup that we were investigating by using pulsed light rather than continuous light. We showed that starting the particle at rest, using a starting nano-unit acceleration stage separation distance of 200 nm and a pulse width of .0016 s gives us a final velocity of 1 m/s after a distance of 65.3 km is traveled. We also showed that the nanoparticle experiences diminishing returns from the applied acceleration of each nano-unit as its velocity increases. The surface plasmon polariton linear nanoparticle accelerator may also have potential for future ground-based research.

Acknowledgments

The authors would like to thank the Air Force Office of Scientific Research for supporting this work. Additionally, J. N. Maser would like to thank the Missouri University of Science and Technology for sponsoring his graduate program.

References

[1]Bradford, J., "2015 SpaceWorks Nano/Microsatellite Market Assessment," SpaceWorks, Atlanta, GA, Jan. 2015.

[2]Juan, M. L., Righini, M., Quidant, R., "Plasmon nano-optical tweezers," *Nature Photonics*, Vol. 5, No. 6, pp. 349-356, 2011.

[3]Rovey, J. L., Friz, P. D., Hu, C., Glascock, M. S., Yang, X., "Plasmonic Force Space Propulsion," *Journal of Spacecraft and Rockets*, Vol. 52, No. 4, pp. 1163-1168, 2015/07/01.

[4]Shoji, T., Tsuboi, Y. "Plasmonic Optical Tweezers toward Molecular Manipulation: Tailoring Plasmonic Nanostructure, Light Source, and Resonant Trapping," *J. Phys. Chem. Lett.*, Vol. 5, pp. 2957-2967., Aug. 14, 2014.

[5]Shalin, A., Sukhov, S., "Plasmonic Nanostructures as Accelerators for Nanoparticles: Optical Nanocannon," *Plasmonics*, Vol. 8, Iss. 2, pp. 625-629, Sep. 11, 2012.

[6]Schmid, G., Corain, B., "Nanoparticulated Gold: Syntheses, Structures, Electronics, and Reactivities," *Eur. J. Inorg. Chem.*, pp. 3081-3098, 2003.

[7]Tsai, W., Huang, J.-S., Huang, C., "Selective Trapping or Rotation of Isotropic Dielectric Microparticles by Optical near Field in a Plasmonic Archimedes Spiral," *Nano Lett.*, Vol. 14, pp. 547−552, 2014.

[8]Grigorenko, A. N., Roberts, N. W., Dickinson, M. R., Zhang, Y., "Nanometric optical tweezers based on nanostructured substrates," *Nature Photonics*, Vol. 2, pp. 365-370, May 11, 2008.